3. Weinhouse S. Glycolysis, respiration and anomalous gene expression in experimental hepatomas. Clows memorial lecture. *Cancer Res* 1972;32:2007–2016.
4. Hatanaka M. Transport of sugars in tumor cell membranes. *Biochim Biophys Acta* 1974;355:77–104.
5. Braams AW, Pruim J, Nikkels GJ. Nodal spread of squamous cell carcinoma of the oral cavity detected with PET-tyrosine, MRI and CT. *J Nucl Med* 1996;37:897–901.
6. Wahl RL, Cody R, Hutchins G, et al. Positron-emission tomographic scanning of primary and metastatic breast carcinoma with the radiolabeled glucose analog 2-deoxy-2-[$^{18}$F]-fluoro-D-glucose [Letter]. *N Engl J Med* 1991;324:200.
7. Sokoloff L, Reivich M, Kennedy C, et al. The [$^{14}$C]deoxyglucose method for the measurement of local cerebral glucose utilization: theory, procedure and normal values in the conscious and anesthetized albino rat. *J Neurochem* 1977;28:897–916.
8. Kuhl DE, Metter EJ, Riege WH. Patterns of local cerebral glucose utilization determined in Parkinson's disease by the [$^{18}$F]fluorodeoxyglucose method. *Ann Neurol* 1984;15:419–424.
9. Kester MV, Phillips TL, Gracy RW. Changes in glycolytic enzyme levels and isoenzyme expression in human lymphocytes during blast transformation. *Arch Biochem Biophys* 1977;183:700–708.
10. Kraaijenhagen RJ, Rijksen G, Staal EJ. Hexokinase isoenzyme distribution and regulatory properties in lymphoid cells. *Biochim Biophys Acta* 1980;631:402–410.
11. Rempel A, Bannasch P, Mayer D. Differences in expression and intracellular distribution of hexokinase isoenzymes in rat liver cells of different transformation stages. *Biochim Biophys Acta* 1994;1219:660–668.
12. Gallagher BM, Fowler JS, Gutterson NI, et al. Metabolic trapping as a principle of radiopharmaceutical design: some factors responsible for the biodistribution of [$^{18}$F]2-deoxy-2-fluoro-D-glucose. *J Nucl Med* 1978;19:1154–1161.
13. Nishioka T, Oda Y, Seino Y, et al. Distribution of the glucose transporters in human brain tumors. *Cancer Res* 1992;52:3972–3979.
14. Brown RS, Wahl RL. Overexpression of GLUT-1 glucose transporter in human breast cancer: an immnohistochemical study. *Cancer* 1993;72:2979–2985.
15. Yamamoto T, Seino Y, Fukumoto A, et al. Overexpression of facilitated glucose transporter genes in human cancer. *Biochem Biophys Res Commun* 1990;170:223–230.
16. Nishioka T, Oda Y, Seino Y, et al. Distribution of the glucose transporters in human brain tumors. *Cancer Res* 1992;52:3972–3979.
17. Mueller-Klieser W, Vaupel P, Manz R, Schmidseder R. Intracapillary oxyhemoglobin saturation of malignant tumors in humans. *Int J Radiat Oncol Biol Phys* 1981;7:1397–1404.
18. Brown JM, Giaccia AJ. Tumor hypoxia: the picture has changed in the 1990s. *Int J Radiat Biol* 1994:65:95–102.
19. Clavo AC, Brown RS, Wahl RL. Fluorodeoxyglucose uptake in human cancer cell lines is increased by hypoxia. *J Nucl Med* 1995;36:1625–1632.
20. Hamacher K, Coenen HH, Stocklin G. Efficient stereospecific synthesis of no-carrier-added 2-[F-18]-fluoro-2-deoxy-D-glucose using aminopolyether supported nucleophilic substitution. *J Nucl Med* 1986;27:235–238.
21. Shetty M, Loeb JN, Ismail-Beigi F. Enhancement of glucose transport in response to inhibition of oxidative metabolism: pre- and posttranslational mechanisms. *Am J Physiol* 1992;262:C527–C532.
22. Klip A, Logan WJ, Li G. Hexose transport in L6 muscle cells. Kinetic properties and the number of [$^{3}$H]cytochalasin B binding sites. *Biochim Biophys Acta* 1982;687:265–280.
23. Polt, R, Porreca F, Szabo L, et al. Glycopeptide enkephalin analogues produce analgesia in mice: evidence for penetration of the blood-brain barrier. *Proc Natl Acad Sci* 1994;91:7114–7118.
24. Gateley SJ. Iodine-123-labeled glucose analogs: prospects for a single-photon-emitting analog of fluorine-18-labeled deoxyglucose. *Nucl Med Biol* 1995;22:829–835.
25. Cartee GD, Douen AG, Ramlal A, et al. Stimulation of glucose transport in skeletal muscle by hypoxia. *J Appl Physiol* 1991;70:1593–1600.
26. Koivisto UM, Martinez-Valdez H, Bilan PJ, et al. Differential regulation of the GLUT-1 and GLUT-4 glucose transport systems by glucose and insulin in L6 muscle cells in culture. *J Biol Chem* 1991;266:2615–2621.
27. Bashan N, Burdett E, Guma A, et al. Mechanisms of adaptation of glucose transporters to changes in the oxidative chain of muscle and fat cells. *Am J Physiol* 1993;264: C430–C440.
28. Mercado CL, Loeb JN, Ismail-Beigi F. Enhanced glucose transport in response to inhibition of respiration in clone 9 cells. *Am J Physiol* 1989;257:C19–C28.
29. Lindholm P, Minn H, Leskine-Kallio S, et al. Influence of the blood glucose concentration on FDG uptake in cancer: a PET study. *J Nucl Med* 1992;34:1–6.
30. Wahl RL, Henry CA, Ethier SP. Serum glucose effects on tumor and normal tissue accumulation of [$^{18}$F]fluoro-2-deoxy-D-glucose (FDG) in rodents with mammary carcinoma. *Radiology* 1992;183:643–647.
31. Knox WE, Jamdar SC, Davis PA. Hexokinase, differentiation and growth rates of transplanted rat tumors. *Cancer Res* 1970;30:2240–2244.
32. Flier JS, Mueckler MM, Usher P, et al. Elevated levels of glucose transport and transporter messenger RNA are induced by *ras* or *src* oncogenes. *Science* 1987;235: 1492–1495.
33. Birnbaum MJ, Haespel HC, Rosen OM. Transformation of fibroblasts by FSV rapidly increases glucose transporter gene transcription. *Science* 1987;235:1485–1498.

# Tumor Metabolic Rates in Sarcoma Using FDG PET

Janet F. Eary and David A. Mankoff
*Division of Nuclear Medicine, University of Washington, Seattle, Washington*

In a busy clinical environment, the arterial blood sampling and long imaging time used for the determination of tumor metabolic rates are not always feasible. In this study, the relationship of tumor standard uptake value (SUV) and metabolic rate of FDG (MRFDG) was investigated in a group of patients with sarcoma. To further investigate the implications of reducing blood sampling requirements for determining tumor metabolic rate, the relationship between FDG blood clearance, obtained from serial venous blood sampling and from a hybrid method of early cardiac blood pool imaging, and late venous blood sampling was analyzed. **Methods:** Comparisons of the sarcoma SUV and MRFDG obtained using graphical analysis, dynamic FDG imaging and venous blood sampling were made. Also, venous and hybrid blood time-activity curves were analyzed for similarity and for their effect on the estimated tumor metabolic rate. **Results:** For this group of patients with sarcoma (n = 42), the tumor SUV and MRFDG had a consistent relationship, with an overall correlation coefficient of 0.94. The MRFDG, determined by venous blood sampling, had a 6% average overestimate, compared to the same value obtained by the hybrid method of early blood pool imaging and late venous sampling. **Conclusion:** Both the correlation of SUV and MRFDG and the hybrid blood pool/tumor imaging protocol provide clinically feasible methods for obtaining tumor metabolic rate information in a busy clinical PET service.

**Key Words:** FDG; sarcoma; PET; metabolic rate

**J Nucl Med 1998; 39:250–254**

A goal of our institution is to provide information on pretreatment tumor grade in sarcoma and to assess response to therapy. Sarcomas present clinically as large masses that are often heterogeneous, and the biological behavior of these tumors is thought to be driven by the highest-grade region of the tumor. The characteristics of this tumor region are the data upon which treatment decision and planning are based. A practical problem that exists in treatment is that biopsy of a small portion of tumor does not yield the overall character of the tumor and may miss those clinically significant high-grade areas.

We proposed that, in our sarcoma tumor population, FDG imaging would provide objective information on the entire tumor and that generation of the local metabolic rate of FDG (MRFDG) of the tumor from dynamic quantitative imaging would improve performance of FDG static imaging and semiquantitative analysis for assessing tumor grade (*1–3*). However, because of the practical problems associated with clinical

Received Sep. 6, 1996; revision accepted Mar. 27, 1997.
For correspondence or reprints contact: Janet F. Eary, MD, University of Washington Medical Center, Division of Nuclear Medicine, Box 356113, Seattle, WA 98195-6113.

quantitative FDG imaging (blood sampling, long imaging time and complex data calculations), we also sought to determine the relationship between simpler, static imaging measures of FDG uptake, such as tumor standard uptake variable (SUV) (*4*) and the MRFDG determined from graphical analysis (*5,6*). Additionally, we had the goal of designing imaging protocols to reduce or eliminate blood sampling, to make FDG quantitative imaging more clinically attractive.

## MATERIALS AND METHODS

### Patients

Patients with either soft tissue or bony sarcomas, presenting to the University of Washington Sarcoma Clinic with primary or recurrent tumors, were selected for quantitative FDG imaging. Patients gave informed consent for the imaging study by signing University of Washington Human Subjects and Radiation Safety Committee approved forms. The 42 patients in this series ranged in age from 22 to 80 yr and had tumors representing all subtypes of soft tissue and bony sarcomas. A total of 65 lesion sites were characterized: 7 benign lesions, 35 untreated malignant lesions and 23 malignant lesions were imaged after chemotherapy. Tumors were located in the extremities (n = 47), torso (n = 17) and head (n = 1). Untreated malignant tumors were classified as high-, intermediate- or low-grade, based on standard pathological criteria from analysis of biopsy or excision of the mass. Twenty of the untreated tumors were high-grade, and 15 were low- or intermediate-grade. All of the patients had renal and hepatic function within normal limits, and none were diabetic.

### PET Imaging

All imaging studies were performed on an Advance Tomograph (General Electric Medical Systems, Waukesha, WI) operating in two-dimensional high-sensitivity mode, with 35 imaging planes covering an axial field of view of 15 cm (4.0 mm axial FWHM at the center of the tomograph) and in-plane resolution of 4–5 mm (*7,8*). An intravenous line was placed in each arm (one side for FDG injection and one side for venous blood sampling). If an indwelling central line was available, it was used for venous blood sampling. Patients were positioned in the tomograph, and a 20- to 30-min attenuation scan over the tumor site was acquired. FDG was prepared using the method of Hamacher et al. (*9*) and had a radiochemical purity of >35 Ci/mmol and specific activity of >1.6 GBg/mmol. FDG (3–10 mCi, or 111–370 MBq) was infused over 2 min with a syringe pump, followed by 60 min of emission scanning. Imaging acquisition times, starting with the beginning of tracer infusion, were as follows: four 20-sec, four 40-sec, four 1-min, four 3-min and eight 5-min intervals. Serial venous blood samples were obtained at 1-min intervals up to 7 min after injection and then progressively less frequently up to 5-min intervals near the end of the 60-min study. Blood samples were centrifuged, and plasma was counted on a Cobra well counter (Packard Instrument Co., Merien, CT). The blood glucose level was determined on the prescan and 30- and 60-min blood samples by a Beckman glucose analyzer (Beckman Instruments, Inc., Brea, CA).

To investigate the use of an alternate imaging protocol to reduce blood sampling requirements, 10 additional patients were imaged using a protocol designed to capture early blood-pool activity from image data. Three patients had tumor sites in which the cardiac blood pool was imaged simultaneously. Seven patients underwent a special imaging protocol that began with transmission images over the chest. Next, using the time binning described previously, dynamic emission images of the chest and cardiac blood pool were obtained, from the start of infusion to 17 min postinfusion. The patient was then positioned in the scanner to image the tumor site from 20 to 60 min after the start of infusion. Patients underwent transmission studies at the tumor site, either before or after injection, correcting for the presence of activity in the patient (*10,11*). In this series, seven patients had sarcomas, two had low-grade lymphomas and one had a squamous cell head and neck cancer.

Images underwent real-time corrections for random coincidences and convolution-based corrections for scattered coincidences (*12*). Tissue time-activity curves (TACs) were generated from the mean region of interest (ROI) value for each image in the dynamic dataset, corrected for the physical decay of $^{18}F$. They were reconstructed onto 128 × 128 matrices covering a 55-cm transaxial field of view, with a Hanning filter with a Nyquist cutoff frequency on a roll-off, resulting in reconstructed resolution of approximately 12 mm (*7,8*). Cross-calibration of image data with blood sample counts was performed on the same day as each study using a 500-ml vial containing $^{18}F$. Vials were imaged on the tomograph, and aliquots of the vial fluid were counted in triplicate on the well counter to determine image calibration factors.

### Image Analysis

In all studies, the 30- to 60-min summed images were used to guide ROI placement. ROIs, ranging in size from 1.3 to 34.5 $cm^2$ (typically, 2–4 $cm^2$) were placed over the tumor on three adjacent 4.25-mm-spaced planes for each subject and included the area with maximal counts on the summed image. Tissue TACs were generated from application of the ROIs to the dynamic image set and corrected for the physical decay of $^{18}F$. SUV for an image region was calculated was follows:

$$SUV = \frac{\bar{A}}{ID/m} \cdot \frac{\text{Plasma glucose}}{100}, \qquad \text{Eq. 1}$$

where $\bar{A}$ is mean tissue activity from 30 to 60 min (in $\mu$Ci/ml), ID is the injected dose (in mCi), m is the patient weight (in kg) and plasma glucose is the average plasma glucose over the study (in mg/dL). The SUV, as described above, performs an empirical correction for plasma glucose (*4*). Metabolic rate of FDG was calculated using the graphical analysis method (*5,6*), described by the following equation:

$$\frac{A}{C_b} = K_i \frac{\int_o^t C_b d\tau}{C_b} + (V_0 + V_b), \qquad \text{Eq. 2}$$

where A is tissue concentration of tracer at any time, $C_b$ is the blood concentration of tracer at any time, $V_0$ and $V_b$ are the tracer volume of distribution and blood partial volume, respectively, and $K_i$ is the tracer blood-tissue transfer constant. $K_i$ is obtained from the slope of the fit of $A/C_b$ versus $\int_o^t C_b d\tau/C_b$ for the time points between 20 and 60 min after injection. The time for each point in the tissue TAC was taken as the center of the time bin. Matched time points in $C_b$ were obtained using linear interpolation between neighboring time points in the measured blood curve. The blood input integral was calculated using trapezoidal integration between interpolated blood TAC points. Using the blood-tissue transfer constant obtained from graphical analysis, the glucose metabolic rate was calculated as follows (*5,13–15*):

$$\text{MRFDG } (\mu\text{mol/min/100 g tissue}) = [\text{Plasma glucose}] \cdot K_i. \qquad \text{Eq. 3}$$

We did not attempt to account for the differences in tissue handling of glucose and FDG; therefore, the quantitative imaging result is expressed as the MRFDG rather than inferred glucose metabolic rate based on an assumed lumped constant.

For the 10 patients for whom heart blood pool was imaged, either because the heart was close to the tumor site or because they were scanned using the chest/tumor site imaging protocol, additional ROI analysis was performed to estimate blood activity from

the left ventricular blood pool image (*16*). A 1.9-cm-diameter circular ROI was placed on three adjacent 4.25-mm-spaced image planes at the base of the left ventricular cavity adjacent to the valve plane, as determined from the early images in which blood pool was well-delineated. Counts from these three regions were summed to generate the blood TAC. The blood pool curve obtained from injection to 17 min was combined with venous blood samples data taken from 20 to 60 min to form a hybrid blood curve. Factors obtained from the calibration vials were used to cross-calibrate image blood pool and blood sample data, and curves were expressed in mCi/ml units. For comparison, each patient also had full venous blood sampling, as described above.

### Data Analysis

For each patient, the tumor MRFDG values and SUVs were plotted, and simple linear regression was performed using a spreadsheet program (Excel, Microsoft Corp., Redmond, WA). The strength of the correlation was judged by the correlation coefficient. Regression analyses were also performed separately for untreated high-grade tumors versus low- or intermediate-grade tumors (determined by pathological analysis) and for high-metabolic activity lesions (MRFDG > mean) and low-metabolic activity lesions (MRFDG < mean).

For the patients who had early blood pool images, additional analyses were performed to determine the range of differences between the arterial and venous curves, as well as the resulting effect on the estimated MRFDG. Each individual curve was normalized by dividing by the mean of the hybrid blood pool/venous curve (mean curve integral divided by total time over which the curve was sampled, typically 60 min). Using the normalized curves, early blood pool and venous curves were compared for all 10 patients. Also, the resulting integral differences between the hybrid and venous curves were calculated, being representative of the difference between arterial and venous curves. Finally, to assess the impact of differences in the hybrid and venous curves on the estimated MRFDG, tumor and normal tissue blood-tissue transfer constants were estimated using both the hybrid blood pool/venous blood curve versus the venous blood curve.

## RESULTS

Examples of the data collected on each study are shown in Figure 1. This shows the complete dataset for analysis. The blood sampling sequence and the image time binning are shown.

Figure 2 shows the relationship between tumor MRFDG and SUV for the entire group of patients studied. This data analysis shows a high correlation ($r = 0.94$, $p < 0.001$) between these two measures of tumor FDG uptake in this patient population. The acquisition of tumor SUV from a simple static image analysis has a consistent quantitative relationship with the MRFDG obtained by graphical analysis (Table 1). The SUV versus MRFDG relationship was further analyzed for high-grade versus intermediate- or low-grade untreated tumors and for high-metabolic activity lesions (MRFDG > mean; mean = 11.7 μmole/min/100 g) versus low-metabolic activity lesions (MRFDG < mean) (Table 1). Correlations are better for high-grade versus lower-grade tumors ($r = 0.94$ versus $r = 0.80$) and for tumors with MRFDG values larger than the mean value ($r = 0.89$ versus $r = 0.62$).

Figure 3 shows the average blood curves and s.d. values for the 10 studies obtained from the hybrid blood pool/venous blood sampling scheme versus venous blood sampling. The plots demonstrate that the cardiac blood pool curve, which approximates an arterial curve, and venous curves merge approximately 20 min after injection. Although the early

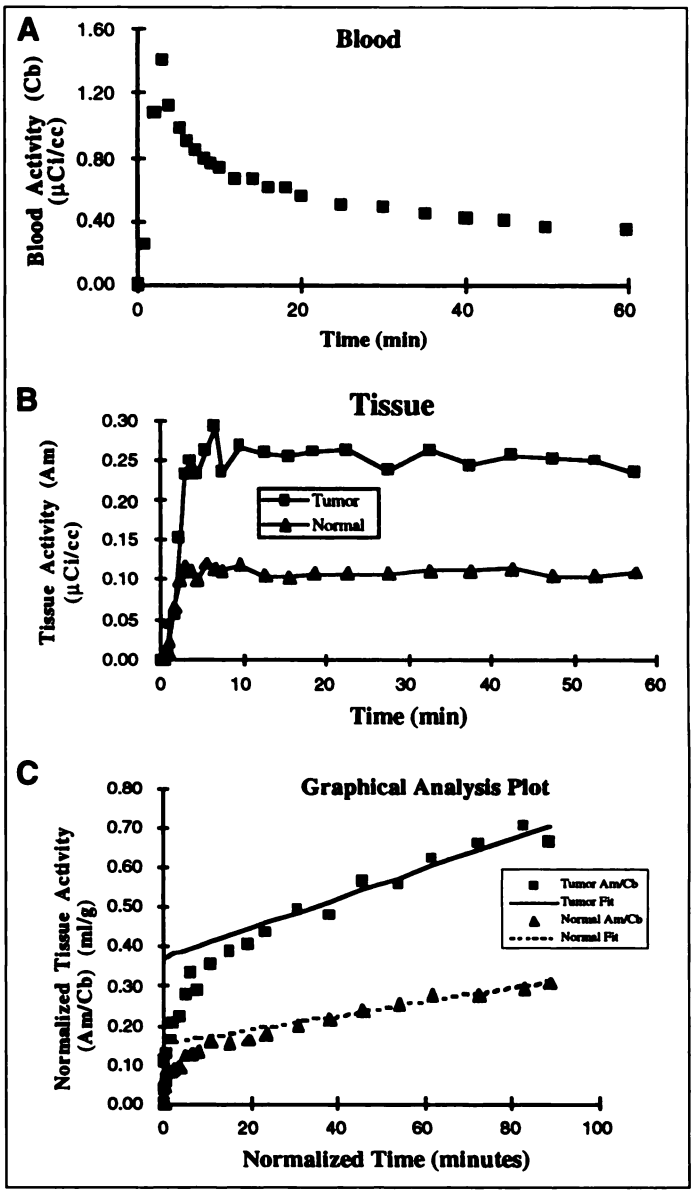


**FIGURE 1.** Sample data obtained from dynamic FDG imaging of a patient with soft-tissue sarcoma. (A) Blood TAC ($C_b$ versus time). (B) Tissue TACs for tumor and normal muscle ($A_m$ versus time). (C) Graphical analysis plots for tumor and normal muscle ($A_m/C_b$ versus normalized time). Regression lines using tissue data obtained 20–60 min after injected are also plotted.

portions of the blood curves differ, the average integral difference from 0 to 60 min after injection for the hybrid versus the venous curve is 10% (range −4% to 20%). One patient with venous sampling through a central venous line had a high early venous blood TAC, leading to an integral 4% higher than the cardiac blood pool curve. Figure 4 shows the MRFDG estimated from the venous sampling versus the hybrid method for 10 tumor regions for the 10 patients and 5 normal muscle regions for the 5 patients with sarcoma and normal muscle in the field of view. The MRFDG estimates obtained using the venous blood curves are an average of 6% higher than those obtained using the hybrid blood curve (range −2% to 14%). There is a consistent relationship between the two: venous MRFDG versus hybrid MRFDG has a slope of 1.10, an intercept of −0.08 and a correlation of 0.9997.

## DISCUSSION

In this series of PET imaging studies in patients with sarcoma, we established our goal of determining the relation-

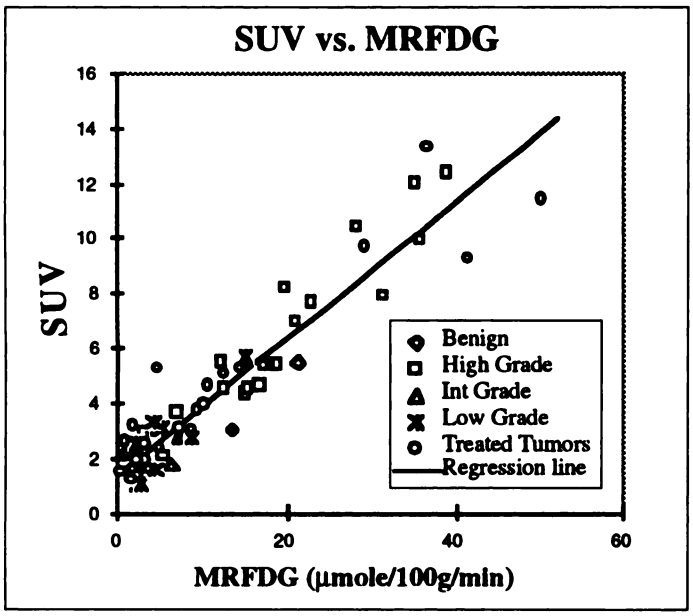


**FIGURE 2.** Plot of SUV versus graphically estimated MRFDG. Linear regression line is shown for reference.

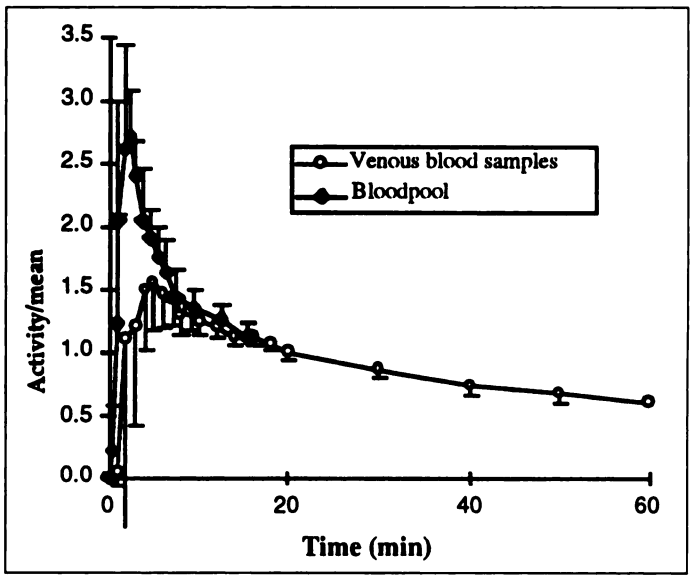


**FIGURE 3.** Average normalized blood TACs obtained using venous blood sampling (○) and early blood pool imaging (◆). Error bars represent s.d. values of individual time points for the 10 studies.

ship between the often maligned SUV (*17*) and the more difficult to obtain MRFDG. With the high degree of correlation in these two values, we can translate the SUV obtained from a simple clinical static PET image of a sarcoma study to the MRFDG. Not surprisingly, the SUV and MRFDG are better correlated for tumors with high metabolic rates, in which a greater portion of the tissue activity is present as metabolically trapped tracer. The correlation is weaker in tumors with lower metabolic rates. In these tumors, MRFDG would be expected to be a more consistent measure of metabolic activity than SUV because a greater portion of the tissue activity results from nonphosphorylated tracer not yet cleared from the tissue. The experience of our group and others in imaging low-grade sarcomas and treated tumors supports this notion (*18–20*).

Several factors contribute to the consistent relationship between SUV and MRFDG. Blood curve analysis in our group of patients demonstrates that the shape of the blood TAC is relatively constant from patient to patient when a standard infusion protocol (2-min infusion) is used in a population of nondiabetic patients with normal hepatic and renal function. Furthermore, SUVs are corrected for plasma glucose. Taken together, these measures resulted in tumor SUVs with a consistent relationship to the MRFDG.

One potential limitation in this analysis is that all tumors included in this study are sarcomas. However, this is a heterogeneous group of tumors, and our data include benign and malignant lesions, as well as tumors before and after treatment. Despite the fact that only one tumor type is represented in this study, the data are from a variety of tumor subtypes and resulted in a wide range of FDG metabolic rates for comparison.

**TABLE 1**
Standard Uptake Value Versus Metabolic Rate of FDG Regression Results

| Category | Slope | Intercept | Correlation | n* |
|---|---|---|---|---|
| All tumors | 0.25 | 1.41 | 0.94 | 65 |
| High-grade untreated tumor | 0.27 | 1.20 | 0.94 | 20 |
| Intermediate- or low-grade untreated tumor | 0.27 | 1.02 | 0.80 | 15 |
| MRFDG, <11.7 μmol/min/100 g | 0.22 | 1.51 | 0.62 | 40 |
| MRFDG, >11.7 μmol/min/100 g | 0.24 | 1.54 | 0.89 | 25 |

*n = number of data points in the regression analysis.

In comparing SUV to MRFDG, we have used graphical estimates using blood TACs obtained through venous sampling rather than arterial sampling, which would be required to measure the true blood input function. However, our analysis comparing results with "arterial" samples obtained from the early cardiac blood pool demonstrate only minimal errors in the estimated MRFDG when venous instead of arterial blood sampling was used. This is, in part, due to the fact that graphical analysis requires only a knowledge of the integral of the early blood curves, as opposed to the exact shape of the early blood curve, which would be important when more detailed rate constant modeling methods are used.

From a practical clinical imaging standpoint, our data analysis suggests that adequate blood TAC data for Patlak analysis can be obtained by venous blood sampling. Therefore, clinically relevant data can be obtained without arterial blood sampling,

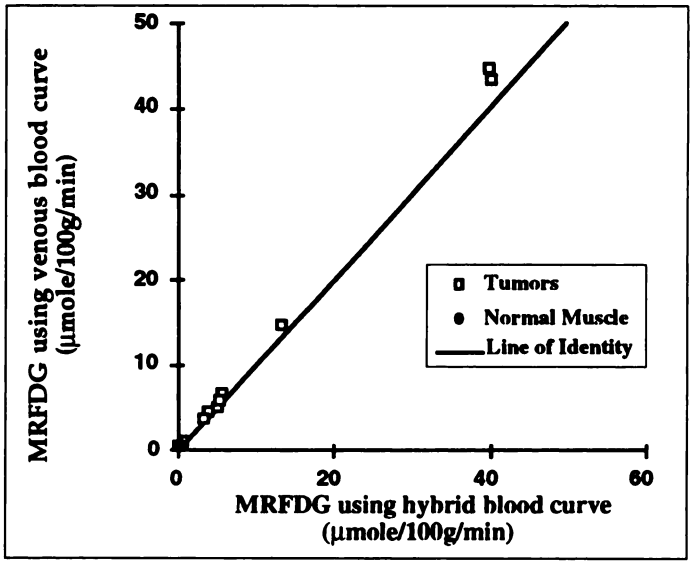


**FIGURE 4.** Plot of MRFDG estimated using venous blood sampling versus MRFDG estimated using the hybrid blood pool/venous sampling scheme. Results are shown for tumor regions (□) and normal muscle (●). Identity line is shown for reference.

which is difficult in routine patient studies, and serial studies in a patient measuring tumor response to therapy. Our results show that an imaging sequence that includes the heart in the field of view in early dynamic imaging and a limited number of venous blood samples thereafter is sufficient to delineate the blood curve necessary to perform graphical estimates of MRFDG. This further reduces blood sampling requirements and makes routine estimation of MRFDG in tumor studies quite manageable. Preliminary investigations by other investigators in our laboratory (*21*) suggest that it may be possible to limit blood sampling even further using patient clinical variables (e.g., weight, height and renal function) and families of blood curves to estimate the blood curve from the limited blood samples.

Overall, these investigations point the way to improved clinical use of quantitative FDG PET to investigate tumor metabolism and response to treatment. Using the methods we have outlined, routine quantitative estimates of tumor glucose metabolism are practical, even in a busy clinical service.

## CONCLUSION

In this data analysis, we established a relationship between the tumor SUV and MRFDG, determined by quantitative imaging and Patlak analysis, for a group of patients with sarcomas. This relationship has a high degree of correlation and can be used clinically to infer the tumor MRFDG from a static FDG PET image. Additionally, the use of limited venous blood sampling and an imaging sequence to capture the early blood input data from the cardiac blood pool is validated for future studies in other tumors and more specific cancer clinical questions.

## ACKNOWLEDGMENTS

This work was supported by National Institutes of Health Grants CA65537 and CA42045. We acknowledge the University of Washington PET Center for assistance in performing the PET tumor imaging studies and the Section of Orthopedic Oncology for patient referrals. We thank Lawrence Durack and Cheryl Vernon for technical assistance, Aaron Charlop for production and quality control of FDG, and Mark Muzi and Dr. Kenneth Krohn for helpful comments.

## REFERENCES

1. Adler L, Blair H, Makley J, et al. Noninvasive grading of musculoskeletal tumors using PET. *J Nucl Med* 1991;32:1508–1512.
2. Kern K, Burnetti A, Norton J, et al. Metabolic imaging of human extremity musculoskeletal tumors by PET. *J Nucl Med* 1988;29:181–186.
3. Griffeth L, Dedashti F, McGuire A, et al. PET evaluation of soft-tissue masses with fluorine-18 fluoro-2-deoxy-D-glucose. *Radiology* 1992;182:185–194.
4. Ichiya Y, Kuwaqbara Y, Otsuka M, et al. Assessment of response to cancer therapy using fluorine-18-fluorodeoxyglucose and positron emission tomography. *J Nucl Med* 1991;32:1655–1660.
5. Patlak C, Blasberg R, Fenstermacher J. Graphical evaluation of blood-to-brain transfer constants from multiple-time uptake data. *J Cereb Blood Flow Metab* 1983;3:1–7.
6. Gjedde A. Calculation of cerebral glucose phosphorylation from brain uptake of glucose analogs in vivo: a re-examination. *Brain Res Rev* 1982;4:237–274.
7. DeGrado T, Turkington T, Williams J, Stearns C, Hoffman J. Performance characteristics of a whole-body PET scanner. *J Nucl Med* 1994;35:1398–1406.
8. Lewellen TK, Kohlmeyer S, Miyaoka R, Schubert S, Stearns C. Investigation of the count rate performance of the General Electric Advance positron emission tomograph. *IEEE Trans Nucl Sci* 1995;42:1051–1057.
9. Hamacher K, Coenen H, Stocklin G. Efficient stereospecific synthesis of no-carrier-added 2-[$^{18}$F]-fluoro-2-D-glucose using aminopolyether supported nucleophilic substitution. *J Nucl Med* 1986;27:235–238.
10. Thompson CJ, Ranger N, Evans AC, Gjedde A. Validation of simultaneous PET emission and transmission scans. *J Nucl Med* 1991;32:154–160.
11. Carson RE, Daube-Witherspoon ME, Green MV. A method for post-injection PET transmission measurements with a rotating source. *J Nucl Med* 1988;29:1558–1567.
12. Bergstrom M, Eriksson L, Bohm C, Blomqvist G, Litton J. Correction for scattered radiation in a ring detector positron camera by integral transformation of the projections. *J Comput Assist Tomogr* 1983;7:42–50.
13. Sokoloff L, Reivich M, Kennedy C, et al. The [$^{14}$C]deoxyglucose method for the measurement of local cerebral glucose utilization: theory, procedure, and normal values in the conscious and anesthetized albino rat. *J Neurochem* 1977;28:897–916.
14. Reivich M, Alavi A, Wolf A, et al. Glucose metabolic rate kinetic model parameter determination in humans: the lumped constant and rate constants for [$^{18}$F]fluorodeoxyglucose and [$^{11}$C]deoxyglucose. *J Cereb Blood Flow Metabol* 1985;5:179–192.
15. Phelps ME, Huang SC, Hoffman EJ, Selin C, Sokoloff L, Kuhl DE. Tomographic measurement of local cerebral glucose metabolic rate in humans with (F-18)2-fluoro-2-deoxy-D-glucose: validation of method. *Ann Neurol* 1979;6:371–388.
16. Weinberg IN, Huang SC, Hoffman EJ, et al. Validation of PET-acquired input functions for cardiac studies. *J Nucl Med* 1988;29:241–247.
17. Keyes J. SUV: standard uptake or silly useless value? *J Nucl Med* 1995;36:1836–1839.
18. Eary J, Conrad E, Bavisotto L, Bruckner J, Howlett A. Determination of sarcoma biologic behavior by quantitative FDG PET imaging. In: *PET and cancer symposium*. Groningen, The Netherlands: 1996;51–52.
19. Eary J, Conrad E, Bavisotto L, Bruckner J, Howlett A. Quantitative FDG PET assessment of sarcoma response to neo-adjuvant chemotherapy. In: *PET and cancer symposium*. Groningen, The Netherlands: 1996;18–19.
20. Nieweg O, Pruim J, van Ginkel R, et al. Fluorine-18-fluorodeoxyglucose PET imaging of soft-tissue sarcoma. *J Nucl Med* 1996;37:257–261.
21. O'Sullivan F, Olshen A, Muzi M, Graham MM, Spence A. Quantitation of cerebral glucose utilization in FDG PET studies without intensive blood sampling [Abstract]. *J Nucl Med* 1996;37:221P.